Journal of Power Sources 191 (2009) 297–303

Contents lists available at ScienceDirect

Journal of Power Sources

journal homepage: www.elsevier.com/locate/jpowsour

Impedance diagnosis of metal-supported SOFCs with SDC as electrolyte

Qiu-An Huang[a,b], Bingwen Wang[a], Wei Qu[c], Rob Hui[c,*]

[a] Department of Control Science and Engineering, Huazhong University of Science and Technology, Wuhan, Hubei 430074, PR China
[b] Faculty of Physics and Electronic Technology, Hubei University, Wuhan, Hubei 430062, PR China
[c] Institute for Fuel Cell Innovation, National Research Council Canada, Vancouver, BC V6T 1W5, Canada

ARTICLE INFO

Article history:
Received 15 January 2009
Received in revised form 4 February 2009
Accepted 4 February 2009
Available online 13 February 2009

Keywords:
Metal-supported SOFC
Equivalent circuit models
Degradation
Impedance

ABSTRACT

Degradation mechanism of the metal-supported SOFCs with NiO–$Ce_{0.8}Sm_{0.2}O_{2-\delta}$($N_iO$–SDC) as anode, SDC as electrolyte, $Sm_{0.5}Sr_{0.5}CoO_3$ (SSCo)–SDC composite as cathode was addressed with an emphasis on metal oxidation and thermal expansion mismatch. The diagnosis was based on an improved equivalent circuit model combined with impedance, microstructure and composition analysis of the cell and cell components. The impedance diagnosis indicates that the high contact resistance is a prominent factor impeding the performance of metal-supported SOFCs at 450–600 °C. The observed oxide scale at the interface between metallic substrate and anode, and, the weak bonding between the electrolyte and the cathode may be responsible for the high contact resistances. Energy-dispersive X-ray spectroscopy (EDX) was applied to analyze the change of surface composition of metallic substrate joined with anode in order to elucidate the formed oxide scale. In addition, based on the improved equivalent circuit model, internal shorting current of the cell due to electronic conduction was evaluated.

1. Introduction

Development of SOFCs has been driven due to their fuel flexibility, high-quality waste heat, and tolerance to carbon monoxide [1]. For their commercialization, there do still exist many challenges to overcome including interfacial reaction prevention, sealing improvement, and cell degradation mitigation due to operation at high temperatures (~1000 °C) [2]. With regard to the above challenges, a drive toward lowering operation temperatures hence pushes an architecture shift from ceramic to metallic supports. Forthcoming metal-supported SOFCs are expected to be competitive in power generation with low cost, high strength, better workability, good thermal conductivity, and quick start-up [3]. The resistance to thermal shock for fast thermal cycles for metal-supported SOFCs has been investigated in the previous literature [4–6]. However, as SOFC supports or interconnects, stainless steels in turn may result in rapid cell degradation due to metal oxidation and thermal expansion coefficient (TEC) mismatch, during cell operation or cell fabrication [7–16]. Therefore, it is a necessary step to prevent/mitigate degradation related to oxidation kinetics and thermal expansion coefficient in the development of metal-supported SOFCs.

Electrochemical impedance spectroscopy (EIS) is recognized as a powerful tool for in situ SOFC diagnosis with high resolution, non-destruction and separability [17]. However, an issue for impedance diagnosis is to balance the straightforward correlation and mathematical tractability for impedance modeling. Equivalent circuit models (ECMs) are regarded as a compromise for the above dilemma [18]. In our previous work, polarization characteristics of metal-supported SOFC have been discussed based on equivalent circuit models under the assumption of pure ionic conducting electrolytes [19]. In order to improve the stability of metal-supported SOFCs, a fundamental understanding of cell degradation mechanism seems to be necessary. In present work, an impedance diagnosis was conducted for the metal-supported cell operating over the temperature range of 450–600 °C in order to investigate the cell microstructure degradation related to metal oxidation and TEC mismatch. ECMs adopted for the above diagnosis application should contain essential parameters such as contact resistance, polarization resistance, electrolyte electron resistance, electrolyte ion resistance, and Nernst voltage. Much previous work, briefly reviewed in the following section, has been devoted to ECMs for mixed ionic–electronic conductors (MIECs) [20–39]; however, none of the existing ECMs completely contain the parameters required by the degradation diagnosis mentioned above. The present work describes an improved ECM allowing to investigate the degradation of metal-supported SOFCs and that includes these parameters.

Therefore, it is expected to gain insight into the degradation mechanism of the metal-supported SOFC with SDC as electrolyte based on the improved ECM combined with impedance, microstructure and composition analysis of the cell and cell com-

* Corresponding author. Tel.: +1 604 221 3111; fax: +1 604 221 3001.
E-mail address: Rob.Hui@nrc-cnrc.gc.ca (R. Hui).

0378-7753/$ – see front matter.
doi:10.1016/j.jpowsour.2009.02.004

ponents. The diagnosis results in this work may lead to possible solutions to prevent/mitigate the cell degradation as well.

2. Experimental

Commercially available porous Hastelloy X alloys were used as metallic substrate. Porosity of Hastelloy X was measured by the Archimedes method and its value was 28.0%. A NiO–SDC (70:30 wt.%) anode layer was deposited on Hastelloy X substrate by suspension plasma spray (SPS). The deposited anode layer was reduced and polished before a SDC electrolyte layer was deposited to a thickness of 30 μm by SPS. No sintering is needed and performed after the anode and the electrolyte deposited by SPS. This is a prominent merit of SPS deposition processes [40]. A $Sm_{0.5}Sr_{0.5}CoO_{3-\delta}$(*SSCo*)–*SDC* (75:25 wt.%) composite cathode was screen-printed on the half-cell, subsequently, the cathode was fired at 800 °C for 2 h. Finally, the anode was reduced once again through gradually increasing the concentration of hydrogen gas at 650 °C. The hydrogen was introduced to the anode with an increased concentration of 20%, 40%, 60%, 80%, and 100% balanced with nitrogen with a flow rate of 100 sccm for 5 h.

For polarization tests, the cell was mounted on an alumina tube using Ceramabond 552 (Aremco). Pt meshes were used as current collectors for both anode and cathode. Electrochemical impedance spectra were recorded from 600 to 450 °C at intervals of 50 °C, with humidified hydrogen as fuel and air as the oxidant. The flow rates of hydrogen and air used for the impedance measurements were 100 sccm, respectively. A Solartron 1260 connected to a Solartron 1480A was used to obtain impedance data over the frequency range of 100 kHz to 0.1 Hz, with perturbation amplitude of 50 mV under open circuit condition. After polarization tests, the cross-sectional microstructure of the cell was examined with a scanning electron microscope (SEM, Hitachi S-3500N). EDX spectroscopy was then applied to analyze the cell interfacial area between the metallic substrate and the anode.

3. An improved equivalent circuit model

3.1. Basic conditions

The following assumptions are made for metal-supported SOFCs with mixed conducting electrolyte to simplify the analysis:

(i) the resistance within the current collector is ignored;
(ii) the metal substrate is a pure electron conductor with certain porosity;
(iii) both fuel and oxidant concentration polarizations are ignored. Only the ohmic polarization and activation polarization are considered;
(iv) electrical conductivities of oxygen-ions and electrons are considered, while the conductivity attributed to electron–holes concentration is neglected due to their lower mobility;
(v) the reaction sites or three phase boundaries (TPBs) are uniformly distributed within both cathode and anode;
(vi) the interfacial layers of electrode/electrolyte are regarded as zero-thickness due to their relatively low thickness compared to the electrolyte/electrode assembly;
(vii) local equilibrium is assumed to prevail at all positions in the system;
(viii) all analysis and discussions are based on the assumption that the whole system already attains steady-state instead of a transient state.

A multi-layer structure with external load R_{load}, as shown in Fig. 1, is used to represent the mobile charge fluxes for the metal-supported SOFC with mixed ionic–electronic conducting electrolyte. The multi-layer structure is composed of metal substrate/porous anode/dense electrolyte/porous cathode, with Pt meshes as current collectors. External current is denoted by I_{ext}, external load resistance by R_{load}, ionic current by I_i, electronic current by I_e, and electrolyte thickness by l. The boundaries I, II, III, IV, and V correspond to the interfaces of current collector/metal substrate, metal substrate/anode, anode/electrolyte, electrolyte/cathode, and cathode/current collector, respectively.

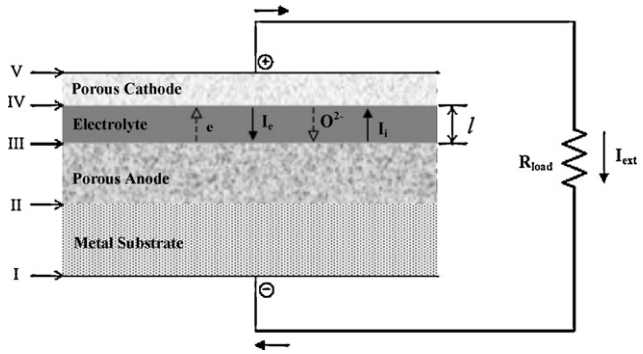

Fig. 1. Schematic illustration of mobile charge fluxes in the metal-supported SOFC with mixed ionic–electronic conducting electrolyte.

If H_2 is used as fuel, the internal electromotive force (e.m.f.) can be expressed as:

$$E_{th} = E^0 - \frac{RT}{2F} \ln \frac{P_{H_2O}}{P_{H_2} P_{O_2}^{1/2}} \quad (1)$$

The ionic transference number of the bulk electrolyte, t_i, can be defined as [41]:

$$t_i = \frac{\sigma_i}{\sigma_t} \quad (2)$$

where σ_i and σ_t denote ionic and total conductivities of the bulk electrolyte, respectively.

The ionic transference number of the bulk electrolyte can be estimated using the following equation:

$$t_i = \frac{V_{ocv}}{E_{th}} \quad (3)$$

where V_{ocv} denotes open circuit voltage.

Under close circuit condition, the correlation of I_{ext}, I_i, and I_e can be expressed as [42]:

$$I_i - I_e = I_{ext} \quad (4a)$$

Under open circuit condition, the net current (or external current), I_{ext}, is zero, i.e.:

$$I_i - I_e = 0 \quad (4b)$$

3.2. Model development

Much work has been done to model impedance for mixed ionic–electronic conductors [20–39]. Jamnik et al. proposed a transfer line model for mixed conductors [28,29]. Subsequently, they further gave the generalized equivalent circuit in which electronic elements were directly correlated to basic materials parameters of SOFCs [30]. These circuit models possess straightforward correlation between model parameters and SOFC parameters; however, they were very complex and difficult to apply. Following Jamnik and Maier's work, Lai and Haile discussed the AC impedance response of the MIEC exposed to a constant chemical potential gradient [31,32]. Liu and Hu redefined the average ionic transference number and gave a simplified ECM of a solid-state cell with mixed conducting

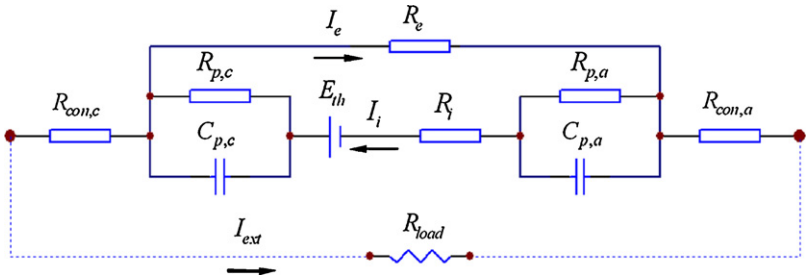

Fig. 2. An equivalent circuit model for the metal-supported SOFC with mixed electronic–ionic conducting electrolyte.

electrolytes [33–35]. Liu and Hu's model, even if easily applicable, still ignored some necessary information, for example contact resistances. Virkar, Kharton, and Marques adopted internal e.m.f. sources instead of capacitances to model the bulk electrolyte and the electrode/electrolyte interfaces in conditions of local equilibrium and electroneutrality [36–39]. Both models considered bulk and interface effects of MIEC with e.m.f. but were mainly suitable for DC situation.

Although great progress and understanding have been made, the balance between the straightforward correlation and mathematical tractability for ECMs, aiming at the degradation diagnosis for SOFCs with mixed conducting electrolytes, still remains unsatisfactory. The absence of such a model is most likely due to the strongly coupled multiple physicochemical processes happening in the cell. As an effort to address the above challenges, an improved ECM, based on previous work [43], is presented. This ECM not only exhibits mathematical tractability but also correlates almost all the necessary information for the degradation analysis. This ECM is shown in Fig. 2. I_i and I_e denote ionic and electronic current through the electrolyte, respectively; R_i and R_e ionic and electronic resistance of the bulk electrolyte, respectively; E_{th} internal e.m.f. source; $R_{p,c}$ and $R_{p,a}$ polarization resistances of the cathode and the anode, respectively; $C_{p,c}$ and $C_{p,a}$ polarization capacitances of the cathode and the anode, respectively; $R_{\text{con},c}$ and $R_{\text{con},a}$ contact resistances attributed to the cathode side and the anode side, respectively; R_{load} external load and I_{ext} external current.

3.3. Model analysis

In DC case, the $C_{p,c}$ and $C_{p,a}$ paths can be treated as open-circuit according to the circuit theory. Based on the equivalent circuit model shown in Fig. 2, the open circuit voltage can be expressed as:

$$V_{\text{ocv}} = \frac{R_e}{R_e + R_i + R_p} \cdot E_{\text{th}} \tag{5}$$

Under open circuit condition ($I_{\text{ext}} = 0$ and $I_i - I_e = 0$), the internal shorting current, I_{short}, can be estimated as:

$$I_{\text{short}} = \frac{E_{\text{th}}}{R_e + R_i + R_p} \tag{6a}$$

and

$$R_p = R_{p,a} + R_{p,c} \tag{6b}$$

where R_p is the cell polarization resistance.

In AC case, E_{th} e.m.f. can be treated as short circuit according to the circuit theory. The complex impedance, $Z(j\omega)$, based on the equivalent circuit model shown in Fig. 2 can be written as:

$$Z(j\omega) = R_{\text{con}} + \frac{R_e(R_i + R_{p,c}/1 + j\omega R_{p,c}C_{p,c} + R_{p,a}/1 + j\omega R_{p,a}C_{p,a})}{R_e + R_i + R_{p,c}/1 + j\omega R_{p,c}C_{p,c} + R_{p,a}/1 + j\omega R_{p,a}C_{p,a}} \tag{7a}$$

and

$$R_T = Z(j\omega)|_{\omega\to 0} = R_{\text{con}} + \frac{R_e(R_i + R_p)}{R_e + R_i + R_p} \tag{7b}$$

and

$$R_{\text{ohm}} = Z(j\omega)|_{\omega\to\infty} = R_{\text{con}} + R_{\text{bulk}} \tag{7c}$$

and

$$R_{\text{bulk}} = \frac{R_e R_i}{R_e + R_i} \tag{7d}$$

and

$$R_{\text{con}} = R_{\text{con},a} + R_{\text{con},c} \tag{7e}$$

where $Z(j\omega)$ denotes cell complex impedance; R_T cell resistance; R_{ohm} cell ohmic resistance; R_{con} cell contact resistance and R_{bulk} bulk resistance of the electrolyte. R_T and R_{ohm} correspond to the intercept of the impedance loop with the real-axis at high frequencies and low frequencies, respectively.

For convenience in the further discussion, an intermediate variable R'_p can be defined as:

$$R'_p = R_T - R_{\text{ohm}} \tag{8}$$

Substituting Eqs. (7b)–(7d) into Eq. (8), we can obtain:

$$R'_p = \frac{R_e(R_i + R_p)}{R_e + R_i + R_p} - \frac{R_e R_i}{R_e + R_i} \tag{9}$$

When $\sigma_i \to 1$ (or), $\sigma_e \to 0$, R'_p turns into R_p, i.e. $R'_p \equiv R_p$, this is only the case for pure ionic conducting electrolytes.

When the polarization resistance is taken into account, as suggested by Liu and Hu [33], the ionic transference number can be re-estimated based on the presented equivalent circuit model as follows:

$$t_i = \frac{V_{\text{ocv}}}{E_{\text{th}}} \cdot \frac{R_e + R_i + R_p}{R_e + R_i} \tag{10}$$

4. Results and discussion

Nyquist plots obtained for the cell under open circuit condition, with moist hydrogen as fuel and dry air as oxidant, over the temperature range of 450–600 °C, are shown in Fig. 3. Detailed test conditions and characterization parameters for the cell are described in previous publications [6,9].

After polarization test, in order to investigate the microstructure degradation, the cell was characterized using a scanning electron microscope. Fig. 4 shows the microstructure of the polished cross-section of the metal-supported SOFC after testing. The micrograph indicates the SDC layer fabricated by suspension plasma spray is completely dense. No macro cracks or continuous pores can be observed across the cross-section of the cell. The interfaces between the electrolyte and the anode and between the metallic substrate

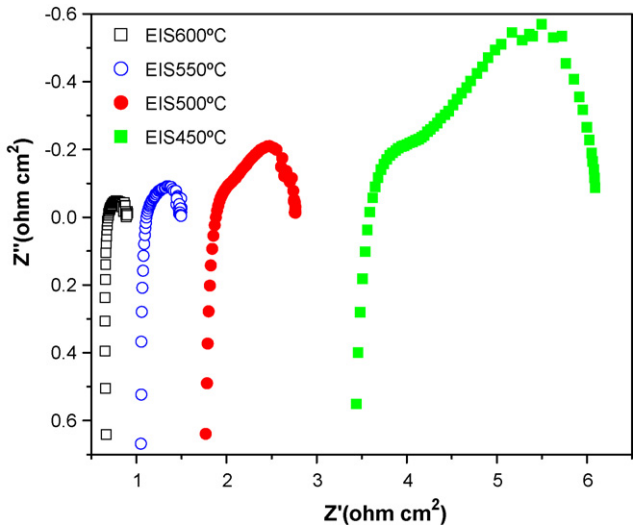

Fig. 3. Electrochemical impedance spectra of metal-supported SOFC under open circuit over the temperature range of 450–600 °C.

and the anode evidence compact contact; in contrast, a weak bonding is observed at the interface between the electrolyte and the cathode.

Cross-sectional SEM images, focused on the interface between the cathode and the electrolyte for the metal-supported cell after testing, can be observed in Fig. 5. According to previous analysis, the weak bonding observed on this micrograph can be attributed to the TEC mismatch across the interface of SDC/SSCo–SDC [6]. The screen-printing deposition method used for the cathode layer is also suspected to contribute to the weak bonding between the cathode and the electrolyte. The large particle is SDC verified by the EDX, which is due to poor dispersion and should be avoided in the future work.

The microstructure at the interface between the metallic substrate and the anode for the metal-supported cell can be observed on Fig. 6. The anode layer shows the desired porous microstructure for gas diffusion, and, an oxide scale is observed at the interface between the metallic substrate and the anode. EDX spectroscopy was applied to three different spots of the cell cross-sectional area, i.e., inside the anode layer, at the interface anode layer/metallic substrate, inside the metallic substrate. The elemental analysis results are summarized in Table 1. As shown in Table 1, the Cr/Fe ratio at interface of the anode and metallic substrate increased by 17%

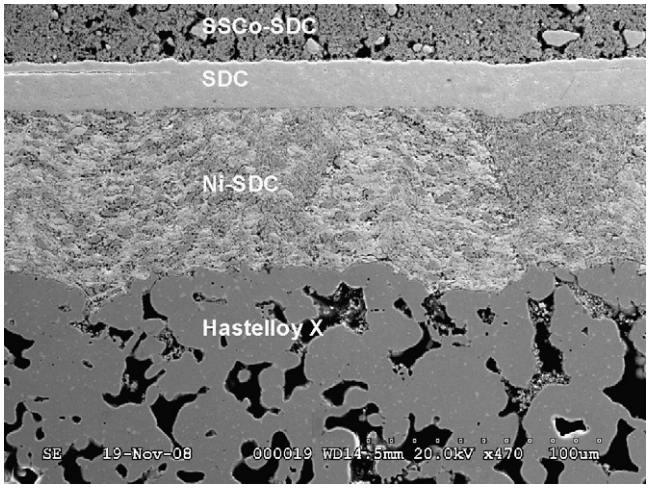

Fig. 4. Cross-sectional SEM image of the metal-supported cell after testing (×470).

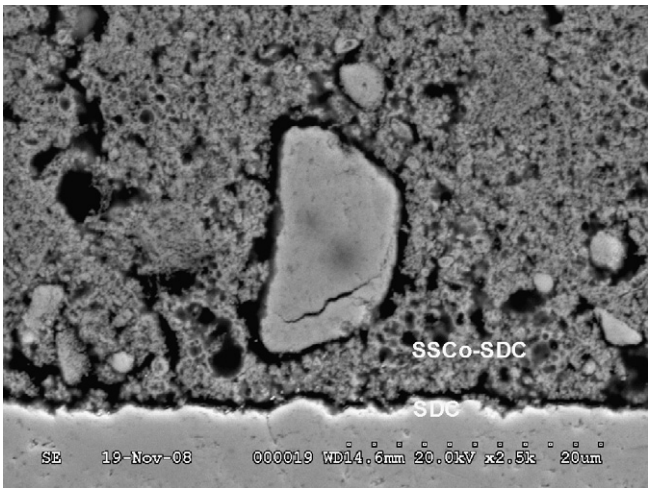

Fig. 5. Cross-sectional SEM image of the interface cathode/electrolyte for the metal-supported cell after testing (×2500).

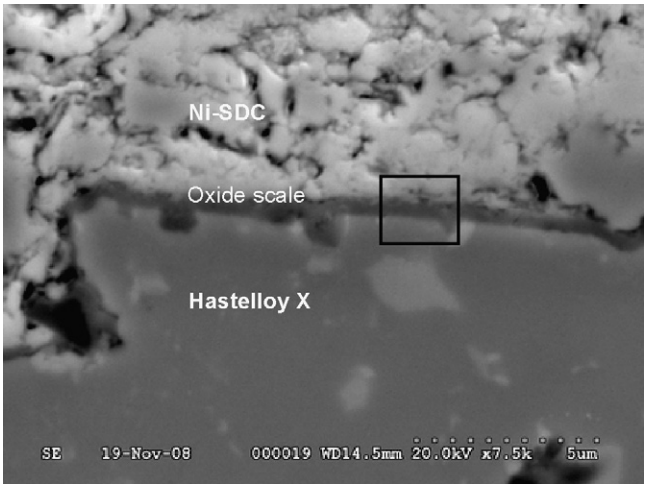

Fig. 6. Cross-sectional SEM image focused on the interface metal/anode of the metal-supported cell after testing (×7500), EDX analysis was located in black pane.

compared to the Cr/Fe ratio in metal. Assuming that Cr-oxides are formed first due to the preferential oxidation of Cr compared to other alloy elements such as Fe, Mo, and Ni, the increase of Cr amount at the interface could be an indication of the existence of Cr-oxide. Just as previously reported [7–11], the diffusion/interdiffusion of chromium, iron, and nickel between metallic substrates and nickel-containing anodes is one of key issues for the degradation of metal-supported SOFCs.

Based on the above measurement and characterization, the diagnosis of the cell degradation was conducted as follows. Cell resistance R_T and cell ohmic resistance R_{ohm} can be extracted from impedance measurements as shown in Fig. 3 over the temperature range of 450–600 °C, then, R'_p can be calculated according to Eq. (8).

Table 1
Elemental analysis results near the interface anode layer/metallic substrate.

Area	Composition (wt.%)			Cr/Fe ratio
	Cr	Fe	Other	
Metal	19.3	24.5	56.2	0.79
Metal/anode interface	11.6	12.1	76.3	0.96
Anode	0	0	100	NA

Table 2
The values of V_{ocv}, E_{th}, and σ_i for the cell.

Temperature (°C)	450	500	550	600
V_{ocv} [a]	0.930	0.905	0.871	0.825
E_{th} [b]	1.186	1.178	1.173	1.168
σ_i [c]	0.0025	0.0064	0.0125	0.0210

[a] Measured values of cell open circuit voltage.
[b] Theoretical values of cell internal e.m.f. [44].
[c] Ionic conductivity of cell bulk electrolyte [45].

The values of V_{ocv}, E_{th}, and σ_i used for the following analysis are summarized in Table 2.

Knowing the electrolyte thickness ($l = 30\,\mu m$), R_i can be estimated according to the expression $R_i = l/\sigma_i$. Consequently, the values of V_{ocv}, E_{th}, R_i, and R'_p over the temperature range of 450–600 °C are all known. Combining Eqs. (5) and (9), R_p and R_e can be estimated using Eqs. (11a) and (11b), respectively

$$R_p = \frac{V_{ocv}E_{th}R'_p - V_{ocv}^2R_i + \sqrt{(V_{ocv}E_{th}R'_p - V_{ocv}^2R_i)^2 + 4V_{ocv}^2E_{th}^2R_iR'_p}}{2V_{ocv}^2} \quad (11a)$$

and

$$R_e = \frac{V_{ocv}(R_p + R_i)}{E_{th} - V_{ocv}} \quad (11b)$$

Subsequently, I_{short}, R_{bulk}, R_{con} and t_i can be estimated according to Eqs. (6a), (7d), (7c) and (10), respectively, based on the measured impedance data, the measured open circuit voltage, and the theoretical value of internal e.m.f. from the previous literatures. These derived results are discussed and shown in Figs. 7–9 as follows.

Fig. 7 shows the variation of ionic transference number t_i, electronic leakage current I_{short}, the theoretical value of internal e.m.f. E_{th}, and measured open circuit voltage V_{ocv} of the cell with SDC electrolyte over the temperature range of 450–600 °C. With the increase of operating temperatures from 450 to 600 °C, t_i decreased from 0.940 to 0.917, I_{short} increased significantly from 0.049 to 0.525 A cm^2, V_{ocv} decreased sharply from 0.930 to 0.825 V. Diagnosis results show that the measured open circuit voltage is lower than the theoretical value of internal e.m.f. mainly due to electronic leakage current, itself being strongly dependant on the temperature [46]. The evolution of t_i, I_{short}, and V_{ocv} with respect to temperature is consistent with previous report [47]. This results also suggest that it is of vital importance to mitigate the electronic leakage current in order to achieve higher output power density and fuel utilization, in particular for metal-supported SOFC with mixed conducting electrolyte operating over 550 °C.

Fig. 8 gives the cell resistance R_T, the cell polarization resistance R_p, and the cell ohmic resistance R_{ohm} over the temperature range 450–600 °C. As expected, R_T, R_p and R_{ohm} decrease with increasing operating temperature. Over 450–600 °C, the values of R_p and R_{ohm} are roughly comparable, suggesting that R_p and R_{ohm} contribute equally to polarization losses of metal-supported SOFC operating at low temperatures.

Fig. 9 shows the contribution of both cell contact resistance and electrolyte bulk resistance to the cell ohmic resistance over the temperature range 450–600 °C. It can be seen that cell contact resistance, R_{con}, is the dominating factor in ohmic polarization losses of metal-supported SOFC. The weak bonding at the interface between the cathode and the electrolyte observed by SEM (Fig. 5) strongly contributes to the high contact resistance $R_{con,c}$; the observed oxide scale, shown in Fig. 6, strongly contributes to the high contact resistance $R_{con,a}$ due to the lower conductivity of the oxide scale compared to the metal substrate or anode bulk [10,48]. Hence, the high R_{con} derived from the impedance diagnosis is an in situ indicator of the cell microstructure degradation. Prevention

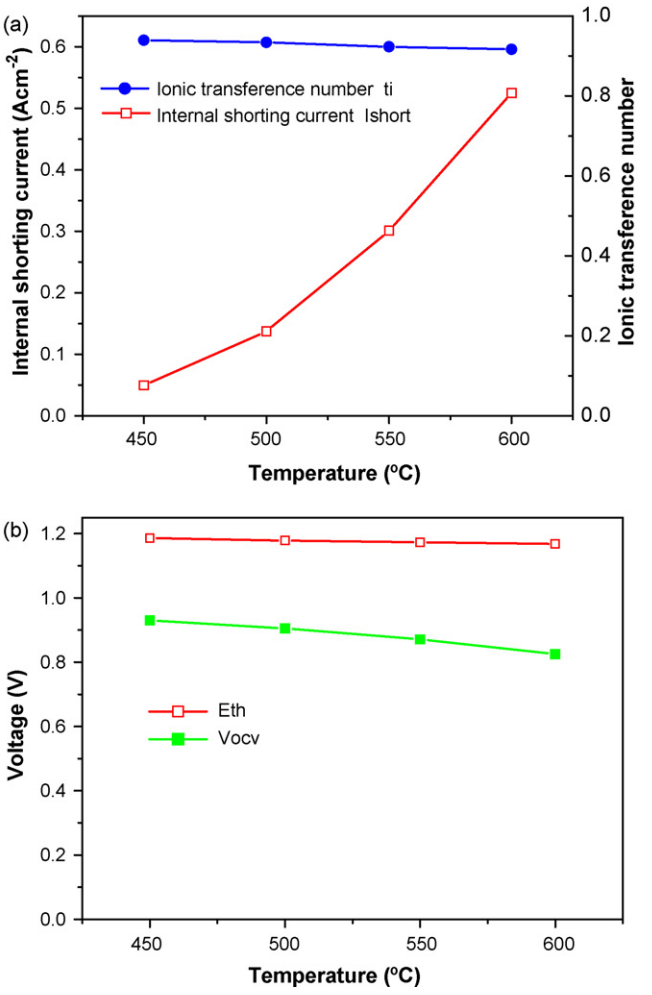

Fig. 7. Analysis of (a) ionic transference number t_i and internal shorting current I_{short} and (b) theoretical open circuit voltage E_{th} and measured open circuit voltage V_{ocv} over 450–600 °C.

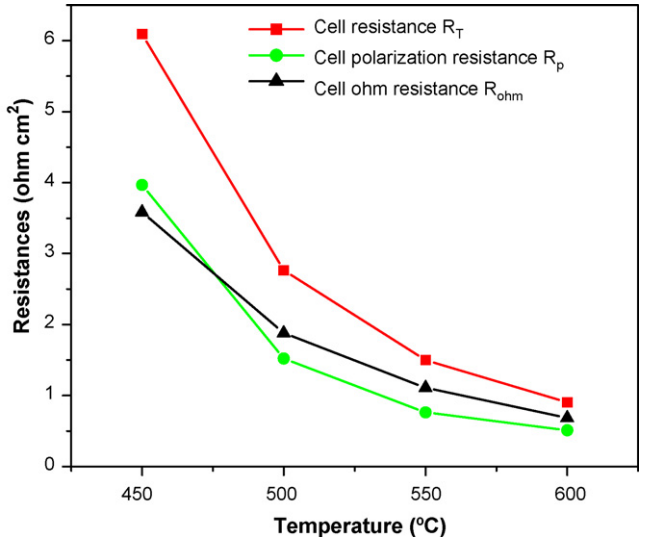

Fig. 8. Analysis of cell resistance, polarization resistance, and ohmic resistance over the temperature range of 450–600 °C.

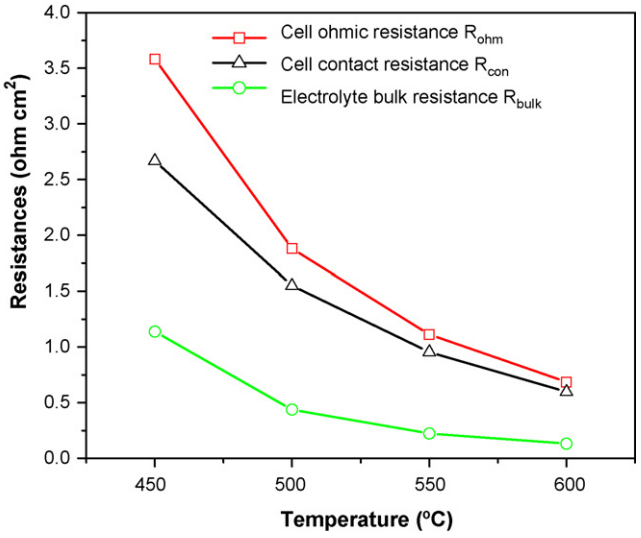

Fig. 9. Analysis of cell ohmic resistance, contact resistance, and electrolyte bulk resistance over 450–600 °C.

of cell microstructure degradation related to metal oxidation and TEC mismatch still represents a challenge for the development of metal-supported SOFCs.

5. Conclusions

Degradation mechanism and electronic leakage current of the metal-supported SOFC with SDC as electrolyte were addressed with an emphasis on metal oxidation and TEC mismatch. It was found that R_p and R_{ohm} contribute equally to polarization loss for low temperature metal-supported SOFC, therefore, both of them should be given equal attention for optimization of cell performance. Metal oxidation and TEC mismatch seems to be responsible for the degradation of metal-supported SOFCs; in other word, the interfacial reaction and the interfacial TEC match of the metal-supported cell are key issues for cell design and optimization. The metal oxidation could be improved by applying a dense conducting ceramic coating, which is similar to the protective coatings for metallic interconnect for cermet-supported SOFCs. Cathode materials not only with high activity but also with the TEC suitable to electrolyte materials should be used in order to improve the stability of the interface between the cathode and the electrolyte. It is of vital importance to eliminate/mitigate the internal shorting current due to electronic conduction in order to improve output power density and fuel utilization for metal-supported SOFCs with mixed conducting electrolytes. This study also demonstrated that the proposed method is valid in diagnosing degradation as well as evaluating electronic leakage current for metal-supported SOFCs with mixed conducting electrolytes. The present ECM could act as an in situ indicator for the degradation phenomena of metal-supported SOFC as discussed in this work. However, the model is invalid under conditions of transient state or load current, especially for large load current due to the simplifying hypothesis for model development.

Acknowledgements

This work was supported by Institute for Fuel Cell Innovation, National Research Council Canada, National Science Foundation of China (No. 60773190), and China Scholarship Council. The authors would also like to thank Jennifer Peron at NRC-IFCI for her proofreading of the manuscript.

Appendix A. Nomenclature

EDX	energy-dispersive X-ray
TEC	thermal expansion coefficient
EIS	Electrochemical impedance spectroscopy
ECM	Equivalent circuit model
MIEC	mixed ionic–electronic conductor
SPS	suspension plasma spray
SEM	scanning electron microscope
TPB	three phase boundaries
e.m.f.	Electromotive force
e	electron
O^{2-}	oxygen ion
t_i	ionic transference number of the bulk electrolyte
l	electrolyte thickness (μm)
R	universal gas constant: $R = 8.314472(15)$ J mol^{-1} K^{-1}
T	Kelvin temperature (K)
F	Faraday constant: $F = 9.64853415(39) \times 10^4$ C mol^{-1}
E_{th}	internal electromotive force (V)
E^0	e.m.f. at standard temperature and pressure, and with pure reactants (V)
V_{ocv}	open circuit voltage (V)
σ_i	ionic conductivity of the bulk electrolyte (s cm^{-1})
σ_t	total conductivity of the bulk electrolyte (s cm^{-1})
I_{ext}	external load current density (A cm^{-2})
I_i	ionic current density of the electrolyte (A cm^{-2})
I_e	electronic current density of the electrolyte (A cm^{-2})
I_{short}	internal shorting current density under open circuit condition (A cm^{-2})
R_{load}	external load area-specific-resistance (ASR) (Ω cm^{-2})
$Z(j\omega)$	cell complex impedance per square centimeter (Ω cm^{-2})
R_i	ionic ASR of the bulk electrolyte (Ω cm^{-2})
R_e	electronic ASR of the bulk electrolyte (Ω cm^{-2})
$R_{p,c}$	polarization ASR of the cathode (Ω cm^{-2})
$R_{p,a}$	polarization ASR of the anode (Ω cm^{-2})
R_p	polarization ASR of the cell (Ω cm^{-2})
$C_{p,c}$	polarization capacitance of the cathode per square centimeter (F cm^{-2})
$C_{p,a}$	polarization capacitance of the anode per square centimeter (F cm^{-2})
$R_{con,c}$	contact ASR attributed from the cathode side (Ω cm^{-2})
$R_{con,a}$	contact ASR attributed from the anode side (Ω cm^{-2})
R_{con}	contact ASR of the cell (Ω cm^{-2})
R_T	total polarization of the cell per square centimeter (Ω cm^{-2})
R_{ohm}	ohmic polarization per square centimeter (Ω cm^{-2})
R_{bulk}	bulk resistance of the electrolyte per square centimeter (Ω cm^{-2})
R'_p	intermediate variable, defined as $R'_p = R_T - R_{ohm}$ per square centimeter (Ω cm^{-2})

References

[1] S.C. Singhal, K. Kendal, High Temperature Solid Oxide Fuel Cells Fundamentals, Design and Applications, Elsevier Ltd., Oxford, England, 2003.
[2] B.C.H. Steel, Solid State Ionics 134 (2000) 3–20.
[3] M.C. Tucker, G.Y. Lau, C.P. Jacobson, L.C. DeJonghe, S.J. Visco, J. Power Sources 171 (2007) 477–482.
[4] Y.B. Matusa, L.C. De Jonghe, C.P. Jacobsonb, S.J. Viscob, Solid State Ionics 176 (2005) 443–449.
[5] M.C. Tucker, G.Y. Lau, C.P. Jacobson, L.C. DeJonghe, S.J. Visco, J. Power Sources 175 (2008) 447–451.
[6] Z.W. Wang, J.O. Berghaus, S. Yick, C. Decès-Petit, W. Qu, R. Hui, R. Maric, D. Ghosh, J. Power Sources 176 (2008) 90–95.
[7] I. Antepara, I. Villarreal, L.M. Rodríguez-Martínez, N. Lecanda, U. Castro, A. Laresgoiti, J. Power Sources 151 (2005) 103–107.
[8] Z.G. Yang, G.G. Xia, G.D. Maupin, J.W. Stevenson, Surf. Coat. Technol. 201 (2006) 4476–4483.

[9] Z.G. Yang, G.G. Xia, M.S. Walker, C.M. Wang, J.W. Stevenson, P. Singh, Int. J. Hydrogen Energy 32 (2007) 3770–3777.
[10] M. Brandner, M. Bram, J. Froitzheim, H.P. Buchkremer, D. Stöver, Solid State Ionics 179 (2008) 1501–1504.
[11] S. Molin, B. Kusz, M. Gazda, P. Jasinski, J. Solid State Electrochem. (2008), doi:10.1007/s10008-008-0635-y.
[12] D.M. England, A.V. Virkar, J. Electrochem. Soc. 148 (2001) A330–A338.
[13] P. Huczkowski, N. Christiansen, V. Shemet, J. Piron-Abellan, L. Singheiser, W.J. Quadakkers, Mater. Corros. 55 (2004) 825–830.
[14] T. Brylewski, J. Dabek, K. Przybylski, J. Therm. Anal. Calorim. 77 (2004) 207–216.
[15] N.P. Brandon, D. Corcoran, D. Cummins, A. Duckett, K. El-Khoury, D. Haigh, R. Leah, G. Lewis, N. Maynard, T. McColm, R. Trezona, A. Selcuk, M. Schmidt, J. Mater. Eng. Perform. 13 (2004) 253–256.
[16] R. Hui, D. Yang, Z. Wang, S. Yick, C. Decès-Petit, W. Qu, A. Tuck, R. Maric, D. Ghosh, J. Power Sources 167 (2007) 336–339.
[17] Q.A. Huang, R. Hui, B. Wang, J. Zhang, Electrochim. Acta 52 (2007) 8144–8164.
[18] J.R. Macdonald, Impedance Spectroscopy—Emphasizing Solid Materials and Systems, John Wiley & Sons, New York, 1987.
[19] Q.A. Huang, J. Berghaus, D.F. Yang, S. Yick, Z.W. Wang, B.W. Wang, R. Hui, J. Power Sources 177 (2008) 339–347.
[20] J.R. Macdonald, J. Chem. Phys. 58 (1973) 4982–5003.
[21] J.R. Macdonald, Electrochim. Acta 37 (1992) 1007–1014.
[22] D.R. Franceschetti, J.R. Macdonald, R.P. Buck, J. Electrochem. Soc. 138 (1991) 1368–1371.
[23] D.R. Franceschetti, Solid State Ionics 70–71 (1994) 542–547.
[24] I. Riess, J. Electrochem. Soc. 128 (1981) 2077–2081.
[25] I. Riess, J. Phys. Chem. Solids 47 (1986) 129–138.
[26] S. Yuan, U. Pal, J. Electrochem. Soc. 143 (1996) 3214–3222.
[27] H. Näfe, J. Electrochem. Soc. 144 (1997) 3922–3929.
[28] J. Jamnik, J. Maier, S. Pejovnik, Electrochim. Acta 44 (1999) 4139–4145.
[29] J. Jamnik, J. Maier, J. Electrochem. Soc. 146 (1999) 4183–4188.
[30] J. Jamnik, J. Maier, Phys. Chem. Chem. Phys. 3 (2001) 1668–1678.
[31] W. Lai, S.M. Hailew, J. Am. Ceram. Soc. 88 (2005) 2979–2997.
[32] W. Lai, S.M. Hailew, Phys. Chem. Chem. Phys. 10 (2008) 865–883.
[33] M. Liu, H. Hu, J. Electrochem. Soc. 143 (1996) L109–L112.
[34] H. Hu, M. Liu, J. Electrochem. Soc. 144 (1997) 3561–3567.
[35] H. Hu, M. Liu, Solid State Ionics 109 (1998) 259–272.
[36] A.V. Virkar, J. Electrochem. Soc. 138 (5) (1991) 1481–1487.
[37] A.V. Virkar, J. Power Sources 147 (2005) 8–31.
[38] A.V. Virkar, J. Power Sources 172 (2007) 713–724.
[39] V.V. Kharton, F.M.B. Marques, Solid State Ionics 140 (2001) 381–394.
[40] R. Hui, Z. Wang, O. Kesler, L. Rose, J. Jankovic, S. Yick, R. Maric, D. Ghosh, J. Power Sources 170 (2007) 308–323.
[41] P.J. Gellings, H.J.M. Bouwmeester, The CRC Handbook of Solid State Electrochemistry, CRC Press, Boca Raton, USA, 1997.
[42] R.T. Leah, N.P. Brandon, P. Aguiar, J. Power Sources 145 (2005) 336–352.
[43] Q.A. Huang, B.W. Wang, Asia-Pacific Power and Energy Engineering Conference, Wuhan, China, in press.
[44] J.H. Joo, G.M. Choi, Solid State Ionics 178 (2007) 1602–1607.
[45] S.W. Zhao, C.R. Xia, G.Y. Meng, J. Power Sources 115 (1) (2003) 44–48.
[46] B.C.H. Steele, A. Heinzel, Nature (London) 414 (2001) 345–352.
[47] X. Zhang, M. Robertson, C. Decès-Petit, W. Qu, O. Kesler, R. Maric, D. Ghosh, J. Power Sources 164 (2007) 668–677.
[48] R. Hui, J. Roller, S. Yick, X. Zhang, C. Decès-Petit, Y. Xie, R. Maric, D. Ghosh, J. Power Sources 172 (2007) 493–502.